The Mechanisms of RNA SHAPE Chemistry

Jennifer L. McGinnis,[†] Jack A. Dunkle,[‡] Jamie H. D. Cate,[‡] and Kevin M. Weeks*,[†]

[†]Department of Chemistry, University of North Carolina, Chapel Hill, North Carolina 27599-3290, United States
[‡]Departments of Chemistry and Molecular and Cell Biology, University of California, Berkeley, California 94720-3220, United States

ⓢ *Supporting Information*

ABSTRACT: The biological functions of RNA are ultimately governed by the local environment at each nucleotide. Selective 2′-hydroxyl acylation analyzed by primer extension (SHAPE) chemistry is a powerful approach for measuring nucleotide structure and dynamics in diverse biological environments. SHAPE reagents acylate the 2′-hydroxyl group at flexible nucleotides because unconstrained nucleotides preferentially sample rare conformations that enhance the nucleophilicity of the 2′-hydroxyl. The critical corollary is that some constrained nucleotides must be poised for efficient reaction at the 2′-hydroxyl group. To identify such nucleotides, we performed SHAPE on intact crystals of the *Escherichia coli* ribosome, monitored the reactivity of 1490 nucleotides in 16S rRNA, and examined those nucleotides that were hyper-reactive toward SHAPE and had well-defined crystallographic conformations. Analysis of these conformations revealed that 2′-hydroxyl reactivity is broadly facilitated by general base catalysis involving multiple RNA functional groups and by two specific orientations of the bridging 3′-phosphate group. Nucleotide analog studies confirmed the contributions of these mechanisms to SHAPE reactivity. These results provide a strong mechanistic explanation for the relationship between SHAPE reactivity and local RNA dynamics and will facilitate interpretation of SHAPE information in the many technologies that make use of this chemistry.
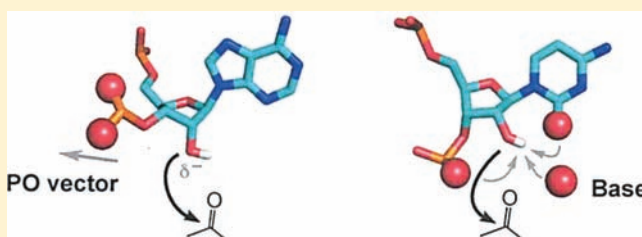
■ INTRODUCTION

The functions of almost all RNAs are governed or tuned by the base-paired secondary structure and higher-order tertiary interactions. Understanding the information expressed in RNA structure thus requires accurate and comprehensive knowledge about the local environment of most nucleotides in an RNA. Selective 2′-hydroxyl acylation analyzed by primer extension (SHAPE) chemistry provides comprehensive information on local nucleotide dynamics and has proven useful in probing structure–function interrelationships in RNA,[1] RNA–protein interactions,[2,3] RNA-small molecule interactions,[4–6] and RNA folding dynamics.[7,8] Because the nucleotide dynamics monitored by SHAPE correlate inversely with the likelihood that a nucleotide is constrained by base pairing, SHAPE data increase the accuracy of RNA secondary structure prediction.[9–12] SHAPE has facilitated development of functional hypotheses in complex biological systems.[13–17] Innovative refinements and applications of SHAPE include time-resolved[7,8,18,19] and temperature-dependent analyses,[5,20] examination of short RNAs[21,22] and interfacing with new readout technologies,[23] detection of long-range through-space interactions,[2,24–27] and identification of optimal sites for attachment of fluorescent reporter probes.[28]

SHAPE reagents are small-molecule electrophiles like 1-methyl-7-nitroisatoic anhydride (1M7)[29] and benzoyl cyanide (BzCN)[18] that react preferentially with the 2′-hydroxyl group of flexible nucleotides to form a 2′-*O*-adduct (Figure 1). The sites at which these adducts form are detected by either primer extension or by protection from exoribonuclease digestion.
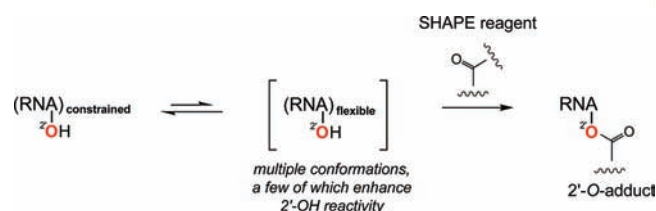

Figure 1. Scheme for SHAPE chemistry emphasizing that reactivity is governed primarily by the ability of a nucleotide to adopt a conformation that enhances the reactivity of the 2′-hydroxyl group toward SHAPE electrophiles.

SHAPE provides a quantitative measure of local nucleotide order,[30] interrogates all four nucleotides in a single experiment,[31] and works well in diverse solution conditions and biological environments.[14,32,33]

The reactivity of the RNA 2′-ribose position is exquisitely sensitive to the nucleotide conformation.[34,35] The mechanism that best explains the quantitative sensitivity of SHAPE to local nucleotide flexibility is that flexible nucleotides sample multiple conformations, and a small number of these conformations enhance the reactivity of the 2′-hydroxyl group toward SHAPE electrophiles (Figure 1). Neither the nature of these reactive conformations nor the mechanisms by which they enhance 2′-OH reactivity are fully understood.
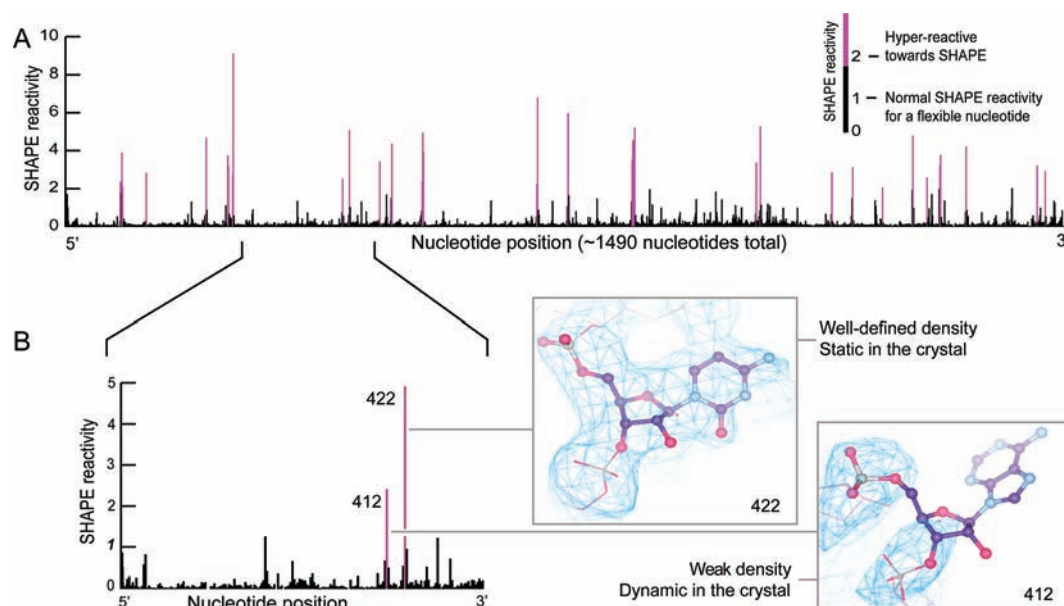
Figure 2. SHAPE chemistry performed on the 16S rRNA in 70S ribosome crystals identifies hyper-reactive nucleotides. (A) SHAPE reactivity histogram. Nucleotides that fall on the conventional SHAPE reactivity scale (normalized nucleotide reactivity <2) are black; nucleotides "hyper-reactive" toward SHAPE reagents are purple. (B) Section of data from panel A showing two hyper-reactive nucleotides. One (nucleotide 412) has poor experimental electron density and is likely dynamic in the crystal, whereas the other (nucleotide 422) has well-defined density. Electron density is drawn at 1σ.

If SHAPE is primarily governed by the ability of a given nucleotide to sample rare conformations that enhance 2′-OH reactivity, then there must exist a few nucleotides that are *constrained* in conformations poised for efficient reaction at the 2′-hydroxyl group. An important first step toward understanding the mechanism of SHAPE was the observation that cyclic adenosine monophosphate (cAMP) is 10- to 18-fold more reactive toward SHAPE reagents than are nucleotides in single-stranded RNA.[35] In the fixed conformation of cAMP, the 3′-phosphodiester is constrained in a 3′,5′ cyclic linkage. The observed "hyper-reactivity" of cAMP is consistent with a model in which close proximity of the negatively charged internucleotide phosphodiester group destabilizes 2′-oxyanion formation during 2′-O-adduct synthesis. It is unlikely, however, that this is the only conformation that enhances the nucleophilicity of the 2′-hydroxyl.

To identify nucleotide conformations that are reactive toward SHAPE, we performed SHAPE on the 16S rRNA in intact crystals of the *Escherichia coli* ribosome.[36] We identified nucleotides that were hyper-reactive relative to the standard SHAPE reactivity scale and that also had well-defined experimental electron density. These nucleotides cluster into a small number of conformations that must facilitate the nucleophilic reactivity of the 2′-hydroxyl toward SHAPE reagents. We explored the mechanisms of these enhancements using a series of nucleotide analogues and showed that 2′-hydroxyl reactivity is enhanced by general base catalysis involving multiple RNA functional group partners and by two specific orientations of the 3′-phosphodiester backbone. These results support specific mechanisms for SHAPE reactivity and will facilitate interpretation of SHAPE reactivities in the many technologies that are now making use of this chemistry.

■ **RESULTS**

In-Crystal SHAPE Reveals Hyper-Reactive Nucleotides. The 1542-nucleotide 16S rRNA in crystals of *E. coli* 70S

ribosomes represents an ideal system to discover the conformations of nucleotides reactive toward SHAPE. First, in the crystal, 16S rRNA is in a static, constrained state; second, individual nucleotides are in diverse conformations; and, third, structural information on nucleotide geometries exists at sufficiently high resolution (3.2 Å) to support development of concrete, testable hypotheses.

Crystals used in SHAPE analyses were essentially identical to those in previous high-resolution structural studies.[36] Before SHAPE probing, the crystals were washed extensively to remove uncrystallized ribosomes. The RNA in the crystals was modified by the addition of 1M7 at 4 °C. After washing to remove ribosomes that might have dissolved as a result of the modification reaction, the RNA was isolated by standard approaches and sites of SHAPE modification were identified by primer extension followed by capillary electrophoresis.[10,37,38]

This analysis yielded a SHAPE reactivity profile for ~1490 of the 1542 nucleotides in the 16S rRNA (Figure 2A). Nucleotide reactivities were normalized to a scale in which unreactive nucleotides had zero reactivity and the mean reactivity of the reactive nucleotides was defined as 1.0. On this scale, reactivities for the vast majority of the nucleotides analyzed fell in a range from 0 to 1.5. However, 35 nucleotides had SHAPE reactivities in the range of 2−10 (in purple, Figure 2A). These hyper-reactive nucleotides presumably adopt conformations that activate the 2′-OH group for the SHAPE reaction. The crystals contain two copies of the ribosome and we focused on the more highly ordered of these (see Methods for additional discussion). In the more ordered ribosome, 17 of the 35 hyper-reactive nucleotides had weak electron density in the crystal structure (Figure 2B, nucleotide 412) and 18 were well-defined by the experimental electron density (Figure 2B, nucleotide 422).

SHAPE Reactivities Are Not Governed by Solvent or Molecular Accessibility. Although all evidence to date suggests that solvent accessibility does not strongly influence

SHAPE reactivity,[1] the in-crystal reactivity profile provided a unique opportunity to evaluate this relationship on a large data set. We compared SHAPE reactivities with the accessibility of the ribose 2′-hydroxyl group as a function of spherical probes ranging from 1.4 to 7.0 Å. The correlation between reactivity and solvent accessibility was low both for a probe size of 1.4 Å ($r = 0.20$) corresponding to water and for one of 6.0 Å ($r = 0.15$), which reflects the approximate molecular diameter of 1M7 (Figure 3). In addition, one-half of the hyper-reactive
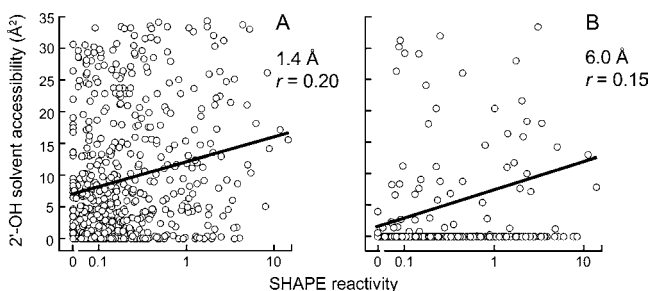

Figure 3. Correlation between SHAPE reactivity and solvent accessibility at the O2′ position for single-stranded nucleotides in the 16S rRNA. Probe sizes of 1.4 and 6.0 Å correspond to the approximate molecular dimensions of water and 1M7, respectively. Pearson's linear r-values are shown.

nucleotides with well-defined conformations (9 of the 18) had low solvent accessibilities, less than 8 Å², at the 2′-hydroxyl position. As many nucleotides with very low solvent and molecular accessibilities reacted readily with 1M7, SHAPE is essentially insensitive to solvent accessibility.

Structural Families for Hyper-Reactive Nucleotides. We grouped the 18 hyper-reactive nucleotides with well-defined conformations in the crystal by structural features, including ribose pucker, distance between 2′-OH and adjacent 3′-phosphodiester, and the presence of a nearby functional or catalytic group. Both the standard C3′-endo and the rarer C2′-endo conformation were represented with 7 and 11 examples, respectively (emphasized in yellow and cyan, Figure 4). Given that nucleotides in the C3′-endo conformation occur roughly 10 times more frequently in RNA than those in the C2′-endo conformation,[39] the C2′-endo conformation is highly over-represented among hyper-reactive nucleotides, a feature noted previously.[32]

The orientation of the 3′-phosphodiester relative to the 2′-OH group was evaluated in two ways: (*i*) as the distance between the 2′-OH and a vector corresponding to the sum of the two phosphorus to nonbridging oxygen bond vectors (see PO-to-2′-OH distance, Figure 5A, top) and (*ii*) as the distance between the 2′-OH and the closest nonbridging phosphate oxygen. Orientations of the 3′-phosphodiester group fell into two distinct conformations. Five nucleotides had orientations in which the nonbridging oxygen groups of the 3′-phosphodiester were oriented *away* from the 2′-OH group, and thus, the PO-to-2′-OH distance was relatively long at ~5.5 Å (Figure 4, left-hand circle). Of these, four were in the C3′-endo conformation and closely resembled the conformation of cAMP (Figure 4, left). This observation supports the model[35] that electrostatic communication between the 3′-phosphodiester and the 2′-OH strongly modulates reactivity of the 2′-hydroxyl group. It is also possible for nucleotides in the C2′-endo conformation to have a long distance between the 3′-phosphodiester and the 2′-OH group; we observed one example in our study (Figure 4, nucleotide A1257). There were 10 examples of the conformation in which one of the nonbridging oxygen groups was within ~3.4 Å of the 2′-OH (Figure 4, right-hand circle). In this case, the nonbridging oxygen likely facilitates SHAPE reactivity by functioning as a general base.

Six nucleotides adopt a conformation that brings the 2′-hydroxyl group within, or very close to, hydrogen bonding
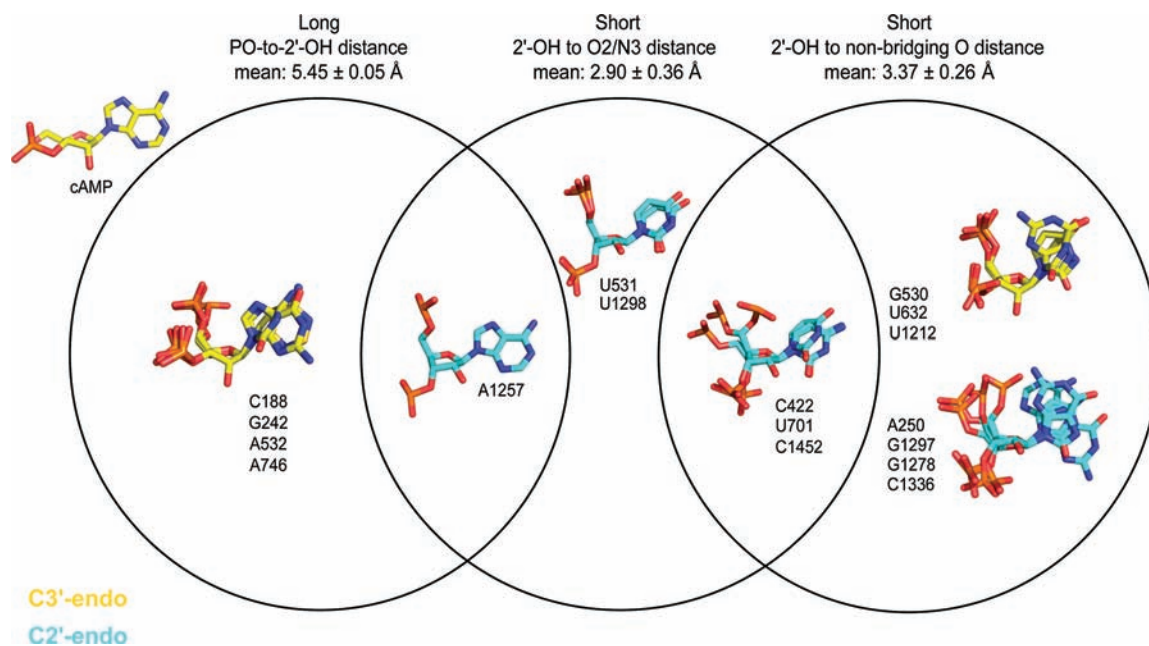

Figure 4. Venn diagram of hyper-reactive nucleotide conformations. Nucleotides in the C3′- and C2′-endo ribose conformations are illustrated in yellow and cyan, respectively. Nucleotides are grouped according to the distance between the 2′-hydroxyl and a vector bisecting the nonbridging oxygen bonds in the 3′-phosphodiester group (see Figure 5A) and proximity of the 2′-hydroxyl to a general base catalytic group. The conformation of hyper-reactive nucleotide A243 does not fall into any of these categories.
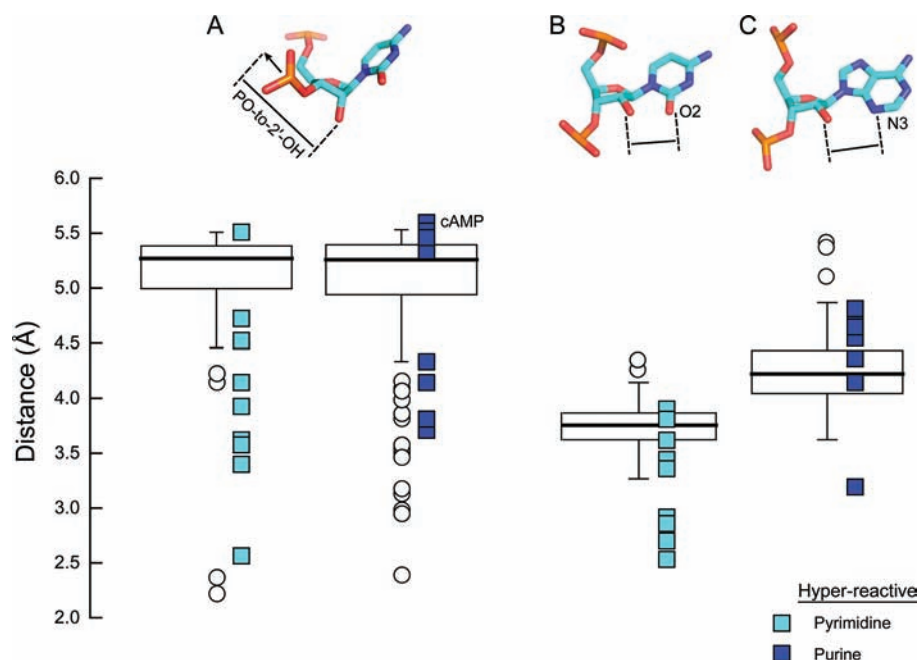
Figure 5. Geometric characteristics of nucleotides hyper-reactive by SHAPE, compared to single-stranded nucleotides with low B-factors in 16S rRNA. Rectangles span the central 50% of the data, the interquartile range, and the median is shown in a heavy line. Whiskers above and below each box give the largest or smallest nonoutlier values; nucleotides with values >1.5 times the interquartile range are shown with circles. Distances for each hyper-reactive pyrimidine and purine nucleotide are shown by colored boxes. (A) Distance between the 2′-OH and the terminus of a vector bisecting the bonds to the nonbridging oxygens in the 3′-phosphodiester. (B) Distance between the 2′-OH and pyrimidine O2. (C) Distance between the 2′-OH and purine N3.

distance of oxygen or nitrogen functional groups with available lone pairs and that might also function as general bases (Figure 4, center circle). In five of these nucleotides, hydrogen bonding between the 2′-OH and the base O2 group of cytosine or uridine was possible, whereas hydrogen bonding with the N3 group of adenosine was possible in one case (A1257). In three examples, the 2′-OH was within 4.2 Å of hydrogen bond acceptors involving nonadjacent nucleotides, suggesting that SHAPE reactivity might be facilitated by long-range, through-space interactions (Supporting Figure 1). Of the 18 hyper-reactive nucleotides, only one, A243, did not fit into any of these conformational categories, and the reason for its hyper-reactivity is not understood.

Hyper-Reactive Nucleotides Have Unusual Conformations. We next evaluated how common the identified conformations are by comparing the geometric parameters of the three classes of hyper-reactive nucleotides to all single-stranded nucleotides in the 16S rRNA with well-defined electron densities (182 nts total). Data are summarized using box plots (Figure 5) in which the rectangle spans the central 50% of the data, or the interquartile range (IQR), and the median is shown as a heavy line. Extreme values, greater than 1.5 times the IQR, are shown explicitly as circle or square symbols. The distribution of PO-to-2′-OH distances (Figure 5A) for the hyper-reactive nucleotides is notably different from that of all single-stranded nucleotides in the 16S rRNA and is distinct for pyrimidine and purine nucleotides. Of the 17 hyper-reactive nucleotides, only one fell into the IQR that characterized most single-stranded nucleotides in 16S rRNA. Five hyper-reactive nucleotides are characterized by a long PO-to-2′-OH distance, possible only when the 3′-phosphodiester points *away* from the 2′-OH group (Figure 5A, top). The remaining 12 hyper-reactive nucleotides showed shorter than

median PO-to-2′-OH distances, consistent with a hydrogen-bonding interaction.

The distribution of distances between the 2′-OH group and the pyrimidine O2 or purine N3 positions is also notably distinct from mean distances between the O2 or N3 position and all 2′-hydroxyl groups in single-stranded nucleotides in the 16S rRNA (Figure 5, panels B and C, respectively). Six of the hyper-reactive pyrimidine nucleotides had much shorter distances between the 2′-OH and the base O2 position than characterized most nucleotides in the 16S rRNA. The distribution among the purine nucleotides was distinct both from single-stranded 16S rRNA nucleotides and from the hyper-reactive pyrimidines. One hyper-reactive purine nucleotide had a short distance between the 2′-hydroxyl and the N3 positions, whereas most of hyper-reactive purine nucleotides had longer than typical distances. These observations suggest that the most favorable conformations that facilitate 2′-OH reactivity may be different for pyrimidine and purine nucleotides. In both cases, enhanced reactivity is strongly favored by an unusual nucleotide conformation.

Functional Group Substitution Supports General Base Catalysis. To test the hypothesis that specific RNA functional groups, especially the nonbridging phosphate oxygen and the pyrimidine O2 group, enhance the nucleophilic reactivity of the 2′-hydroxyl, we evaluated the effect of substituting individual functional groups in the context of a model RNA hairpin with a GNRA tetraloop and a single bulged nucleotide of either A or U. Two nucleotides flanking the 5′ and 3′ sides of the stem were designed to remain unpaired to permit normalization of SHAPE profiles (Figure 6A). In-solution SHAPE indicated that none of the nucleotides in this RNA were hyper-reactive (Figure 6, black lines at right).
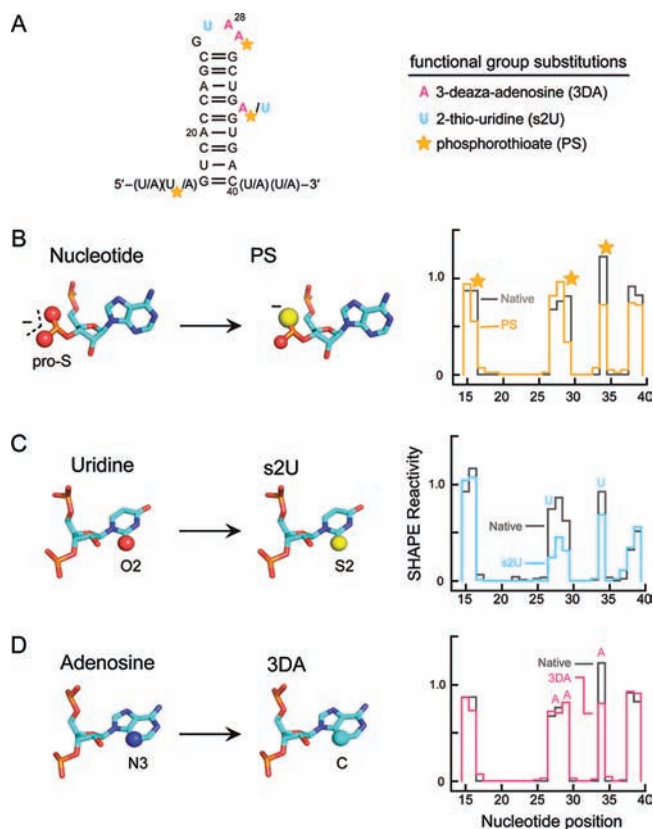
Figure 6. Effects of functional group substitutions on SHAPE reactivity. (A) Structure of the stem-loop RNA showing sites of nucleotide analogue incorporation during transcription. The bulged-A RNA contained flanking U sequences, and vice versa. (B−D) For each substituted transcript, modifications are illustrated on the left and SHAPE reactivities for the modified (colored lines) compared to the unmodified transcript (black lines) are shown on the right. (B) 3′-Phosphorothioate (PS), (C) 2-thio-uridine (s2U), and (D) 3-deaza-adenosine (3DA) functional group substitutions.

In the context of this model, we evaluated the impact of the nonbridging oxygen groups from the 3′-phosphodiester by analysis of a transcript containing phosphorothioate-substituted guanosine analogues. In this RNA, the pro-R oxygen was replaced with sulfur at the 3′-phosphodiester group for three single-stranded residues (Figure 6A, yellow stars). In a standard nucleotide, the phosphate atom and nonbridging oxygens carry a net negative charge, whereas in the phosphorothioate analogue, the charge resides preferentially on the sulfur atom[40] leaving the pro-S oxygen electron deficient and a weaker hydrogen bond acceptor and general base (Figure 6B, left). SHAPE profiles for the native and phosphorothioate-substituted RNAs were similar, indicating that the stem-loop RNA folds into roughly the same structure in both RNAs. Strikingly, however, the SHAPE reactivities at each single-stranded nucleotide with a 3′-phosphorothioate substitution were 2-fold lower than the reactivities of these nucleotides in the unmodified transcript (Figure 6B, graph). The electronic distribution at the 3′-phosphodiester group thus has a significant facilitating effect on 2′-OH reactivity.

The contribution of the pyrimidine O2 group to SHAPE reactivity was evaluated by substitution of the O2 atom with sulfur using 2-thio-uridine (Figure 6C). Sulfur is a poor-hydrogen bond acceptor due to its size and diffuse electron cloud.[41] The thiocarbonyl group in 2-thio-uridine thus disrupts

the ability of this position to serve as a general base. SHAPE reactivities at U27 in the loop and at the bulged U34 in the 2-thio-uridine transcript decreased by 2-fold compared to reactivities of these nucleotides in the unsubstituted RNA (Figure 6C). SHAPE reactivities for the two adenosine nucleotides in the loop, adjacent to U27, also decreased in the 2-thio-uridine-substituted RNA relative to those in the unmodified transcript suggesting that substitution of the O2 position affects the reactivity of neighboring nucleotides.

Finally, the contribution of the purine N3 position was tested using the nucleotide analogue 3-deaza-adenosine (Figure 6D), which substitutes carbon for nitrogen and eliminates the ability of the substituted nucleotide to act as a general base. This substitution caused a 40% decrease in SHAPE reactivity at the bulged A relative to the unmodified RNA but did not change the reactivity of the two adenosines in the loop. These data suggest the purine N3 group facilitates 2′-OH reactivity in some, but not all, structural contexts.

Catalysis by a Solution-Phase General Base. SHAPE reactivity was strongly enhanced by general base catalysis involving functional groups in RNA (Figures 4 and 6). An exogenous solution-phase base should therefore also enhance SHAPE reactivity. We monitored SHAPE reactivity of a 5′-labeled dinucleotide of adenosine and dideoxycytosine, which contains a single free 2′-hydroxyl that reacts with 1M7 to form a mono 2′-O-adduct (Figure 7A). SHAPE reactivity was
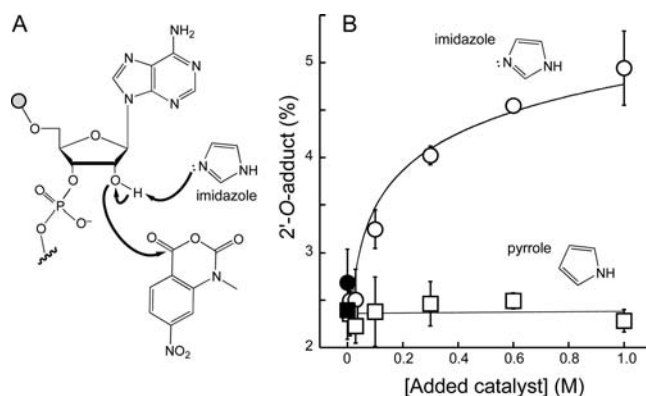

Figure 7. Effect of a solution-phase catalyst on SHAPE adduct formation. (A) Mechanism for general base catalysis of the reaction of a 2′-hydroxyl with SHAPE reagents as mediated by imidazole. (B) Imidazole- versus pyrrole-mediated enhancement of 2′-O-adduct formation.

monitored at constant pH as a function of added imidazole, which contains lone pair electrons on nitrogen and is a good general base. Pyrrole, with a similar structure but without nonbonded lone pairs, was used as a control. Addition of 1 M imidazole increased 2′-O-adduct formation 2-fold, whereas pyrrole addition had no detectable effect on reactivity (Figure 7B). These results strongly support the hypothesis that SHAPE reactivity is enhanced by general base catalysis involving both intranucleotide and through-space catalytic groups.

■ DISCUSSION

RNA SHAPE chemistry detects local nucleotide flexibility in a way that correlates closely with independent measures of molecular order in RNA[30,35] but that is largely independent of solvent or molecular accessibility (Figure 3). SHAPE is best explained by a model in which reactive nucleotides

preferentially sample relatively rare conformations that increase the nucleophilic reactivity of the 2′-OH group (Figure 1). The corollary to this model, which provides a critical segue into understanding the mechanism of SHAPE, is that there must exist a few nucleotides that are constrained in reactive conformations.

Thirty-five nucleotides (~2% of those examined) in the 16S rRNA in crystals of *E. coli* ribosomes proved to have unusually high reactivities when interrogated by SHAPE *in crystallo*. This prevalence of hyper-reactive nucleotides corresponds closely to that observed in prior studies in our laboratory.[9,20] The conformations of 18 of these nucleotides were well-defined by the experimental electron density. Analysis of the conformations adopted by these nucleotides supports two overarching models for the underlying mechanism of SHAPE chemistry.

First, reactivity was enhanced by conformations in which the nonbridging oxygen atoms from the adjacent 3′-phosphodiester are directed *away* from the reactive 2′-OH group. This mechanism was initially characterized using cAMP,[35] which remains one of the most hyper-reactive nucleotides identified to date: Its reactivity is ~15 on the scale used here for 16S rRNA (see Figures 2A and 4). The phosphodiester-away mechanism is now supported by five examples of hyper-reactive nucleotides in the 16S rRNA (Figure 4, left-hand circle). This conformation supports 2′-OH reactivity by reducing electrostatic destabilization of the reactive 2′-oxyanion (δ^-), and perhaps other partial charges, in the transition state (Figure 8A).
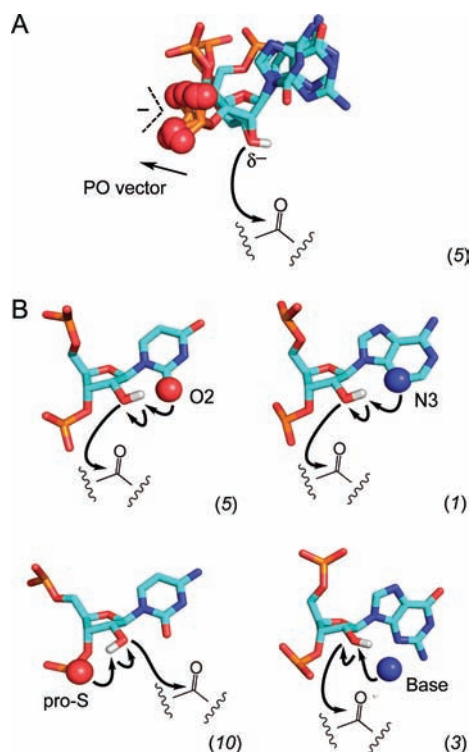

Figure 8. Mechanisms of RNA SHAPE chemistry. (A) Stabilization of the intermediate reactive 2′-oxyanion. In the five superimposed hyper-reactive nucleotides, the nonbridging oxygen groups of the backbone (and the permanent charge) are directed *away* from the 2′-OH group. (B) General base catalysis. Examples of catalysis by the pyrimidine O2, purine N3, pro-S oxygen, and through-space groups are shown. For each panel, the number of occurrences observed in SHAPE analysis of 16S rRNA *in crystallo* is given in parentheses.

Second, SHAPE reactivity was enhanced by a proximal functional group capable of forming a hydrogen bond with the 2′-OH group (Figure 4, middle and right-hand circles). These hyper-reactive conformations are remarkably diverse and include those that allow interactions with functional groups on the nucleobases, the pro-S nonbridging phosphate oxygen, and through-space hydrogen bond acceptors (Figure 8B). In these cases, SHAPE reactivity is facilitated through deprotonation of the reactive 2′-OH via general base catalysis (equivalent to lowering the pK_a of the 2′-OH group). This mechanism is strongly supported by functional group substitution studies showing that reducing the electron density on these atoms, which limits their ability to function as general bases, had a large effect on 2′-OH reactivity (Figure 6).

The vast majority of nucleotides (85) in the 16S rRNA crystal that exhibited high (0.7–2.0) SHAPE reactivities had very little electron density and are likely dynamic. Only 18 nucleotides with high reactivities had well-defined positions in the crystal. Of these, 15 adopted conformations consistent with our reactivity-facilitating conformations (Supporting Table S1). Thus, SHAPE reactivity mechanisms defined by evaluating hyper-reactive positions appear to apply broadly to RNA nucleotides.

When general base catalysis predominates, pyrimidine and purine nucleotides may react via different preferred conformations. The interaction between the pyrimidine O2 and 2′-OH appears to be especially favorable and occurred in five examples in our set of hyper-reactive nucleotides (Figure 4). For purine nucleotides, it appears to be more common for a nonbridging phosphodiester oxygen to function as the general base rather than the 2′-OH (of which we have a single example). Supporting this hypothesis, substitution of the pyrimidine O2 atom had a larger compromising effect on SHAPE reactivity than did substitution at the purine N3 group (Figure 6C,D).

C2′-endo nucleotides were highly over-represented among the hyper-reactive nucleotides, a feature noted in studies of the *Tetrahymena* P546 domain.[32] All examples of apparent intranucleotide general base catalysis involved nucleotides in the C2′-endo conformation (Figure 4, center circle). Our data are consistent with a model in which the C2′-endo conformation facilitates 2′-OH reactivity primarily because it enhances the ability of the 2′-OH group to interact favorably with nearby general base groups, especially with the pyrimidine O2 or purine N3 atoms. However, the C2′-endo conformation is clearly not required for efficient SHAPE reactivity as evidenced by the many examples of hyper-reactive nucleotides in the C3′-endo conformation and by the high reactivity of cAMP, which is constrained in a C3′-endo-like conformation.

Finally, interactions with *nonadjacent* nucleotides can play a significant role in the nucleophilic reactivity of the 2′-OH group. First, phosphorothioate and 2-thio-uridine substitutions affected the reactivity of 2′-OH groups located one or two nucleotides away from the site of the substitution (Figure 6B,C). Second, in addition to local interactions, three 2′-OH groups among the hyper-reactive nucleotides and 11 of 18 2′-OH groups among highly reactive nucleotides are close to a general base group located on a nonadjacent nucleotide in the 16S rRNA (Supporting Figure S1 and Table S1). Third, the strong facilitating effect of imidazole indicates that through-space interactions can significantly enhance 2′-OH reactivity (Figure 7). The net effect of all potential nonadjacent contributions provides a likely explanation for why SHAPE is

uncorrelated with solvent accessibility (Figure 3). Any accessibility penalty born by buried nucleotides is apparently compensated for by the density of functional groups able to function as general base catalysts in a folded RNA.

In sum, SHAPE reactivity at the 2′-OH group is facilitated by two major mechanisms (Figure 8), each of which can be achieved by wide variety of nucleotide conformations. All hyper-reactive conformations identified through our analysis are incompatible with canonical Watson−Crick base pairing and fall predominantly into three well-defined structure classes. That diverse conformations facilitate reactivity strongly reinforces the basic biophysical model that SHAPE measures RNA *dynamics*. The data reported here explain the strong observed correlation between SHAPE reactivity and molecular motion.[30] In addition to understanding SHAPE-based analyses, the specific reactivity mechanisms established here emphasize the broad catalytic potential of functional groups in RNA and provide mechanistic insight into the general reactivity of distinct RNA conformations toward chemical probes, epigenetic modifying agents, and mutagens.

■ METHODS

SHAPE Analysis of 16S rRNA in 70S Crystallized Ribosomes. Crystals of the *E. coli* 70S ribosome were prepared as described.[36] Ribosome crystals were washed three times in the same buffer used for cryo-protection and stabilization in the crystallographic studies, with the exception that the pH was increased from 4.8 to 6.5 [XB: 7% 2-methyl-2,4-penanediol, 7% PEG 8000, 24% PEG 400, 3.8 mM MgCl$_2$, 380 mM NH$_4$Cl, 5.5 mM putrescine, 5 mM spermidine, 22.5 mM MES (pH 6.5)] to remove free ribosomes prior to SHAPE analysis. Crystals were resuspended in 36 μL of XB and SHAPE experiments were initiated by addition of 1/10 vol 1M7 (20 mM) in dimethyl sulfoxide (DMSO). Control reactions contained an equivalent volume of neat DMSO. Reactions were incubated for 2.5 h at 4 °C (approximately 5 half-lives for the hydrolysis rate of 1M7 in XB). Modified crystals were washed three times with XB to remove any free ribosomes, dissolved in 250 μL of 1× TE and 50 μL of 0.1 M dithiothreitol, and extracted three times with phenol/chloroform/isoamyl alcohol (25:24:1) and two times with chloroform/isoamyl alcohol (24:1). Total RNA was recovered by precipitation with ethanol, and 2′-O-adducts were detected by primer extension. Five primer pairs of 19−22 nucleotides were used with 3′ positions complementary to 16S rRNA positions 323, 559, 947, 1112, and 1492.[9] Primer extension products were resolved on an ABI 3130 capillary electrophoresis instrument. As judged from the long extensions obtained, RNA modification to form 2′-O-adducts was sparse, roughly 1 in ~300 nt were modified. Raw electropherograms were analyzed using ShapeFinder.[37] Positions exhibiting high background were discarded and reactivities slightly less than zero were reset to zero. Three independent experiments were completed for each primer set and the resulting SHAPE data averaged (Supporting Figure S2). Data sets were normalized by first excluding the top 2% of reactive nucleotides and then by dividing the reactivity for each nucleotide by the average of the next 8% most reactive nucleotides. The full data set has been deposited in the SNRNASM database.[42]

Analysis of Nucleotide Geometries in 16S rRNA. All analyses started with the well-ordered *E. coli* ribosome visualized in a recent atomic-resolution structure, pdb id 3i1m.[36] The crystals contain two ribosomes in each asymmetric unit. We focused our analysis on the better ordered (A) ribosome. For the nucleotides with well-defined conformations in both ribosome structures, nucleotide conformations were identical. Hyper-reactivities are likely to be underestimated as they reflect contributions from both highly ordered and less well-ordered ribosomes. The starting model was initially improved using MolProbity[43] to identify all-atom clashes and suspect ribose sugar conformations. Corrections were carried out in Coot.[44] Changes to the structure were only accepted if they survived refinement and did not compromise model geometry. The local conformations of nine of the well-ordered hyper-reactive nucleotides were ultimately adjusted (positions 250, 422, 531, 532, 701, 1278, 1297, 1336 and 1452). Nucleotides were initially aligned through the ribose moiety and then grouped according (i) to the distance between the 2′-OH and the vector bisecting the nonbridging oxygens in the adjacent 3′-phosphodiester and (ii) to the presence of a nearby functional group resulting in three categories (Figure 4). One nucleotide (A243) did not fit into any of these three categories as determined by nonparametric box-plot analysis[45] and Dixon's Q-test.[46] For the box-plot analysis (Figure 5), well-ordered single-stranded nucleotides were defined as those not participating in conserved Watson−Crick base pairs, according to the secondary structures derived by comparative sequence analysis,[47] and possessing an atomic displacement factor less than 60 in crystallographic refinement.

Nucleotide Triphosphate Analogues and RNA Stem-Loop Synthesis. Phosphorothioate triphosphates and 2-thiouridine-5′-triphosphate were obtained from Glen Research and Trilink Biotechnologies, respectively. 3-Deaza-adenosine triphosphate was synthesized from 3-deaza-adenosine (Texas Biochemicals) as described.[48] DNA templates directing synthesis of the stem-loop RNA [5′-(U/A)(U/A)GUC ACCAG CGUAA GCUG(A/U) GUGAC (U/A)(U/A)-3′] embedded in 5′ and 3′ structure cassette sequences[35] were obtained by PCR. For analysis of phosphorothioate or 3-deaza-adenosine substitutions, the RNA contained a bulged adenosine and flanking uridine residues; for the 2-thiouridine substitution, the RNA contained a bulged uridine and flanking adenosine residues (Figure 6). RNA constructs were synthesized by *in vitro* transcription [0.5 mL; 40 mM Tris (pH 8.0), 10 mM MgCl$_2$, 10 mM dithiothreitol, 2 mM spermidine, 0.01% (v/v) Triton X-100, 4% (w/v) poly(ethylene) glycol 8000, 2 mM each NTP, PCR-generated template, T7 RNA polymerase; 37 °C; 4 h]. Unsubstituted and nucleotide analogue-containing RNAs were synthesized using 0.1 and 0.2 mg/mL T7 RNA polymerase, respectively. RNAs were separated on a denaturing polyacrylamide gel (1× TBE, 8% polyacrylamide, 7 M urea, 29:1 acrylamide/bisacrylamide, 0.4 mm × 28.5 cm × 23 cm; 35 W, 1.5 h). Bands containing RNA were excised from the gel, and the RNA was recovered by overnight passive elution at 4 °C, followed by precipitation with ethanol. RNAs were resuspended in TE and stored at −20 °C.

SHAPE of the GUAA Stem Loop. RNAs (5 pmol) in 5 μL of 1/2× TE were heated at 95 °C for 2 min, snap-cooled on ice, combined with 3 μL of 3.3× folding buffer [333 mM Hepes (pH 8.0), 333 mM potassium chloride (pH 8.0), and 33 mM MgCl$_2$], and incubated at 37 °C for 20 min. SHAPE experiments were initiated by adding 9 μL of the refolded RNA to 1 μL of 100 mM 1M7 (in DMSO) or neat DMSO. Reactions were incubated at 37 °C for 2 min. SHAPE adducts were detected by primer extension and quantified using Shape-Finder.[37] Data sets were normalized by dividing the value for each nucleotide by the average of the three most reactive nucleotides (10% of the total). SHAPE data sets for the native and analogue-containing RNAs were then rescaled to the identical, single-stranded sequences in the flanking structure cassettes; SHAPE reactivities of these nucleotides were not affected by nucleotide analogue incorporation.

SHAPE Reactivity As a Function of Added Base. The [^{32}P]-labeled adenosine-dideoxy cytosine (pAp-ddC; 1 μL, 100 000 cpm/μL) was incubated for 5 min at 37 °C in 8 μL of 1.25× reaction buffer [62.5 mM HEPES (pH 8.0), 125 mM sodium chloride, 12.5 mM MgCl$_2$] containing either imidazole or pyrrole at 0, 0.0375, 0.125, 0.375, 0.750, or 1.25 M (at pH 8.0). Adduct formation was initiated by adding 9 μL of pAp-ddC-containing solution to 1 μL of 100 mM 1M7 (in DMSO) or neat DMSO. Reactions were incubated for 2 min at 37 °C. Reactions were diluted with 10 μL of H$_2$O and 20 μL of formamide; 2 μL of the resulting solution was subjected to electrophoresis (1× TBE, 30% polyacrylamide; 29:1 acrylamide/bisacrylamide; 0.4 mm × 28.5 cm × 23 cm, 35 W, 1 h); bands were quantified by phosphorimaging.

6623

dx.doi.org/10.1021/ja2104075 | *J. Am. Chem. Soc.* 2012, 134, 6617−6624

■ ASSOCIATED CONTENT

S **Supporting Information**

Figures illustrating hyper-reactive nucleotides for which the facilitating general base is located on a nonadjacent nucleotide and median and standard deviations for the complete in-crystal data set. This material is available free of charge via the Internet at http://pubs.acs.org.

■ AUTHOR INFORMATION

Corresponding Author
weeks@unc.edu

Notes
The authors declare no competing financial interest.

■ ACKNOWLEDGMENTS

■ REFERENCES

(1) Weeks, K. M.; Mauger, D. M. *Acc. Chem. Res.* **2011**, *44*, 1280−1291.
(2) Duncan, C. D.; Weeks, K. M. *Biochemistry* **2008**, *47*, 8504−8513.
(3) Mayerle, M.; Bellur, D. L.; Woodson, S. A. *J. Mol. Biol.* **2011**, *412*, 453−465.
(4) Dann, C. E., III; Wakeman, C. A.; Sieling, C. L.; Baker, S. C.; Irnov, I.; Winkler, W. C. *Cell* **2007**, *130*, 878−892.
(5) Stoddard, C. D.; Gilbert, S. D.; Batey, R. T. *RNA* **2008**, *14*, 675−684.
(6) Wang, B.; Wilkinson, K. A.; Weeks, K. M. *Biochemistry* **2008**, *47*, 3454−3461.
(7) Mortimer, S. A.; Weeks, K. M. *Proc. Natl. Acad. Sci. U.S.A.* **2009**, *106*, 15622−15627.
(8) Lu, C.; Smith, A. M.; Ding, F.; Chowdhury, A.; Henkin, T. M.; Ke, A. *J. Mol. Biol.* **2011**, *409*, 786−799.
(9) Deigan, K. E.; Li, T. W.; Mathews, D. H.; Weeks, K. M. *Proc. Natl. Acad. Sci. U.S.A.* **2009**, *106*, 97−102.
(10) Low, J. T.; Weeks, K. M. *Methods* **2010**, *52*, 150−158.
(11) Bindewald, E.; Wendeler, M.; Legiewicz, M.; Bona, M. K.; Wang, Y.; Pritt, M. J.; Le Grice, S. F.; Shapiro, B. A. *RNA* **2011**, *17*, 1688−1696.
(12) Washietl, S.; Hofacker, I. L.; Stadler, P. F.; Kellis, M. *Nucleic Acids Res.* **2012**, DOI: 10.1093/nar/gks009.
(13) Costantino, D. A.; Pfingsten, J. S.; Rambo, R. P.; Kieft, J. S. *Nat. Struct. Mol. Biol.* **2008**, *15*, 57−64.
(14) Watts, J. M.; Dang, K. K.; Gorelick, R. J.; Leonard, C. W.; Bess, J. W., Jr.; Swanstrom, R.; Burch, C. L.; Weeks, K. M. *Nature* **2009**, *460*, 711−716.
(15) Liang, R.; Kierzek, E.; Kierzek, R.; Turner, D. H. *Biochemistry* **2010**, *49*, 8155−8168.
(16) Gherghe, C.; Lombo, T.; Leonard, C. W.; Datta, S. A.; Bess, J. W., Jr.; Gorelick, R. J.; Rein, A.; Weeks, K. M. *Proc. Natl. Acad. Sci. U.S.A.* **2010**, *107*, 19248−19253.
(17) Grohman, J. K.; Kottegoda, S.; Gorelick, R. J.; Allbritton, N. L.; Weeks, K. M. *J. Am. Chem. Soc.* **2011**, *133*, 20326−20334.
(18) Mortimer, S. A.; Weeks, K. M. *J. Am. Chem. Soc.* **2008**, *130*, 16178−16180.
(19) Mortimer, S. A.; Weeks, K. M. *Nat. Protoc.* **2009**, *4*, 1413−1421.
(20) Wilkinson, K. A.; Merino, E. J.; Weeks, K. M. *J. Am. Chem. Soc.* **2005**, *127*, 4659−4667.
(21) Turner, K. B.; Yi-Brunozzi, H. Y.; Brinson, R. G.; Marino, J. P.; Fabris, D.; Le Grice, S. F. *RNA* **2009**, *15*, 1605−1613.
(22) Steen, K. A.; Malhotra, A.; Weeks, K. M. *J. Am. Chem. Soc.* **2010**, *132*, 9940−9943.
(23) Lucks, J. B.; Mortimer, S. A.; Trapnell, C.; Luo, S.; Aviran, S.; Schroth, G. P.; Pachter, L.; Doudna, J. A.; Arkin, A. P. *Proc. Natl. Acad. Sci. U.S.A.* **2011**, *108*, 11063−11068.
(24) Badorrek, C. S.; Weeks, K. M. *Nat. Chem. Biol.* **2005**, *1*, 104−111.
(25) Reymond, C.; Levesque, D.; Bisaillon, M.; Perreault, J. P. *Structure* **2010**, *18*, 1608−1616.
(26) Legiewicz, M.; Zolotukhin, A. S.; Pilkington, G. R.; Purzycka, K. J.; Mitchell, M.; Uranishi, H.; Bear, J.; Pavlakis, G. N.; Le Grice, S. F.; Felber, B. K. *J. Biol. Chem.* **2010**, *285*, 42097−42104.
(27) Kladwang, W.; Cordero, P.; Das, R. *RNA* **2011**, *17*, 522−534.
(28) Soulière, M. F.; Haller, A.; Rieder, R.; Micura, R. *J. Am. Chem. Soc.* **2011**, *133*, 16161−16167.
(29) Mortimer, S. A.; Weeks, K. M. *J. Am. Chem. Soc.* **2007**, *129*, 4144−4145.
(30) Gherghe, C. M.; Shajani, Z.; Wilkinson, K. A.; Varani, G.; Weeks, K. M. *J. Am. Chem. Soc.* **2008**, *130*, 12244−12245.
(31) Wilkinson, K. A.; Vasa, S. M.; Deigan, K. E.; Mortimer, S. A.; Giddings, M. C.; Weeks, K. M. *RNA* **2009**, *15*, 1314−1321.
(32) Vicens, Q.; Gooding, A. R.; Laederach, A.; Cech, T. R. *RNA* **2007**, *13*, 536−548.
(33) Wilkinson, K. A.; Gorelick, R. J.; Vasa, S. M.; Guex, N.; Rein, A.; Mathews, D. H.; Giddings, M. C.; Weeks, K. M. *PLoS Biol.* **2008**, *6*, e96.
(34) Chamberlin, S. I.; Merino, E. J.; Weeks, K. M. *Proc. Natl. Acad. Sci. U.S.A.* **2002**, *99*, 14688−14693.
(35) Merino, E. J.; Wilkinson, K. A.; Coughlan, J. L.; Weeks, K. M. *J. Am. Chem. Soc.* **2005**, *127*, 4223−4231.
(36) Zhang, W.; Dunkle, J. A.; Cate, J. H. D. *Science* **2009**, *325*, 1014−1017.
(37) Vasa, S. M.; Guex, N.; Wilkinson, K. A.; Weeks, K. M.; Giddings, M. C. *RNA* **2008**, *14*, 1979−1990.
(38) McGinnis, J. L.; Duncan, C. D.; Weeks, K. M. *Methods Enzymol.* **2009**, *468*, 67−89.
(39) Murray, L. J.; Arendall, W. B.,, III; Richardson, D. C.; Richardson, J. S. *Proc. Natl. Acad. Sci. U.S.A.* **2003**, *100*, 13904−13909.
(40) Frey, P. A.; Sammons, R. D. *Science* **1985**, *228*, 541−545.
(41) Donohue, J. *J. Mol. Biol.* **1969**, *45*, 231−235.
(42) Rocca-Serra, P.; Bellousov, S.; Birmingham, A.; Chen, C.; Cordero, P.; Das, R.; Davis-Neulander, L.; Duncan, C. D.; Halvorsen, M.; Knight, R.; Leontis, N. B.; Mathews, D. H.; Ritz, J.; Stombaugh, J.; Weeks, K. M.; Zirbel, C. L.; Laederach, A. *RNA* **2011**, *17*, 1204−1212.
(43) Richardson, J. S.; Schneider, B.; Murray, L. W.; Kapral, G. J.; Immormino, R. M.; Headd, J. J.; Richardson, D. C.; Ham, D.; Hershkovits, E.; Williams, L. D.; Keating, K. S.; Pyle, A. M.; Micallef, D.; Westbrook, J.; Berman, H. M. *RNA* **2008**, *14*, 465−481.
(44) Emsley, P.; Cowtan, K. *Acta Crystallogr., Sect. D: Biol. Crystallogr.* **2004**, *60*, 2126−2132.
(45) Tukey, J. W. *Exploratory Data Analysis*; Addison-Wesley: Reading, MA, 1977.
(46) Rorabacher, D. B. *Anal. Chem.* **1991**, *63*, 139−146.
(47) Cannone, J. J.; Subramanian, S.; Schnare, M. N.; Collett, J. R.; D'Souza, L. M.; Du, Y.; Feng, B.; Lin, N.; Madabusi, L. V.; Muller, K. M.; Pande, N.; Shang, Z.; Yu, N.; Gutell, R. R. *BMC Bioinf.* **2002**, *3*, 2.
(48) Gillerman, I.; Fischer, B. *Nucleosides, Nucleotides Nucleic Acids* **2010**, *29*, 245−256.